Dynamic Modeling of Near Isothermal Compressor for Transcritical Carbon Dioxide Cycle

Haopeng LIU[1], Vikrant AUTE[2]*, Yunho HWANG[3], Chengyi LEE[4],
Jan MUEHLBAUER[5], Lei GAO[6]

[1,2,3,4,5,6]Center for Environmental Energy Engineering
Department of Mechanical Engineering, University of Maryland
College Park, MD 20742 USA
Email: [1]hliu1220@umd.edu, [2]vikrant@umd.edu, [3]yhhwang@umd.edu,
[4]cylee@umd.edu, [5]muehlie@umd.edu, [6]leigao@umd.edu

*Corresponding Author

ABSTRACT

Compressors are the major energy consumption components in vapor compression systems, drawing much research effort in reducing carbon emissions. The isothermal compressor integrates the compressor chamber and gas cooler to achieve near isothermal compression, reaching up to 30% energy reduction compared to the traditional isentropic compression work. This paper presents a detailed isothermal compressor model combined with a generalized liquid piston model to account for the carbon dioxide (CO_2) isothermal compression process. The model is established based on MATLAB environment. The model uses the real experimental data as boundary conditions and initial settings, which also considers the CO_2 solubility in liquid piston (mineral oil) for designing, optimizing and customizing the compression chambers. The validation was carried out with experimental data using a prototype with 3.5 kW capacity. The results have demonstrated the accuracy of the dynamic model (6.2% relative error for chamber pressure and 0.5 K deviation for chamber temperature), which provide a guideline for designing and customizing the isothermal compression cycle.

1. INTRODUCTION

Vapor compression system (VCS) account for more than 30% of total electricity consumption in the U.S. (EIA, 2022), while the compressor consumes the majority of energy within the VCS. Therefore, measures to improve the energy efficiency of VCS, especially during the compression process, play a critical role in the transition to a more sustainable and resilient energy economy.

The isothermal compression can lead the system close to the Carnot cycle efficiency and the related technology have achieved breakthrough progress in past few decades, which can be broadly categorized into three groups such as refrigeration applications, air compression applications and miscellaneous (Kim et al., 2022). Among these, the air compression applications, or in particular, compressed air energy storage (CAES) applications has become a more prevalent option due to the increasing penetration of renewable energy and high storage capacity. Furthermore, majority of the related applications used liquid piston for air compression. For example, Qin and Loth (2014) combined water spray with liquid piston to investigate near isothermal compression, a detailed thermodynamic model was developed and validated with experimental data. The results showed that the total surface area of aloft droplets is critical to achieving high performance in a liquid piston. With the similar test rig, Patil et al. (2020) implemented parametric studies to investigate the isothermal efficiency by varying the injection pressures of spray, spray nozzle angles and stroke time of compression. Experimental results demonstrated that isothermal efficiency consistently increases with the increased injection pressure of spray.

On the other hand, the goal of reducing greenhouse gas emissions is the major driver to mitigate the climate change and many of the refrigerants utilized in VCS are potent greenhouse gases. In view of long-term environmental safety, one potential substitute refrigerant is carbon dioxide (CO_2), a natural refrigerant that has negligible impact on climate

change, which is also non-toxic, non-flammable and non-corrosive. Besides, technological and manufacturing improvements make it possible to achieve high pressure required for CO_2 transcritical operation and the CO_2 systems have been successfully commercialized into automotive air conditioning (Yin et al., 2021, Song et al., 2022), heat pump water heater (Nawaz et al., 2018, Wang et al., 2022) as well as refrigeration system (Karampour and Sawalha, 2018). Unlike the conventional heat pump, where heat rejection occurs through condenser, in transcritical CO_2 heat pump, it happens via single-phase sensible cooling through the gas cooler, therefore, the large pressure difference and uniqueness of gas cooling process need to be addressed.

In addition, the CO_2 solubility in oil is a key parameter during the CO_2 flooding process. The high solubility of CO_2 may bring potential damage to pump since the bubbling occurring during the decompression process may decrease the oil viscosity and accelerate the machines wearing out (Kim, 2022). The correlation that can accurately predict the CO_2 solubility is thereby significant, which not only facilitates the selection of potential candidates of oil with low solubility but also better estimate the charge level within the system during operation.

A key prerequisite for successful implementation of isothermal compression process relies on the heat transfer enhancement strategies to guarantee the efficient heat dissipation and maintain the desired isothermal compression conditions. Besides, the discontinuity of refrigerant flow within the cycle (especially the delivery of CO_2 from isothermal compressor), as well as the control issues also pose challenges to the modeling phase. In this paper, an isothermal compressor model combined with liquid piston is presented, the liquid piston acts as a coolant for the working fluid to maintain optimal operating conditions within the compression chamber and achieve certain cooling capacity for the system. The experimental tests were carried out with the 1-ton refrigeration system and the validated model offers a pure software solution to guide the future design and prototyping. To the authors' knowledge, this is the first development of transient platform for the near isothermal compression transcritical CO_2 refrigeration system.

2. DESCRIPTIONS OF TEST UNIT AND EXPERIMENTAL RIG

Figure 1 shows the corresponding experimental setup of isothermal compressor with a rated cooling capacity of 1 ton. The compression chambers (consists of 4 identical microchannel heat exchangers) were numbered as "chamber 1" and "chamber 2" to realize the double-acting mechanism and are placed in parallel to ensure the even refrigerant distribution during the compression/ suction process. The stainless-steel tank is utilized to ensure the rated load, which didn't involve the heat transfer during the system operation. The plunger pump provides high-pressure liquid to the compression chamber and is designed for the high volumetric efficiency.

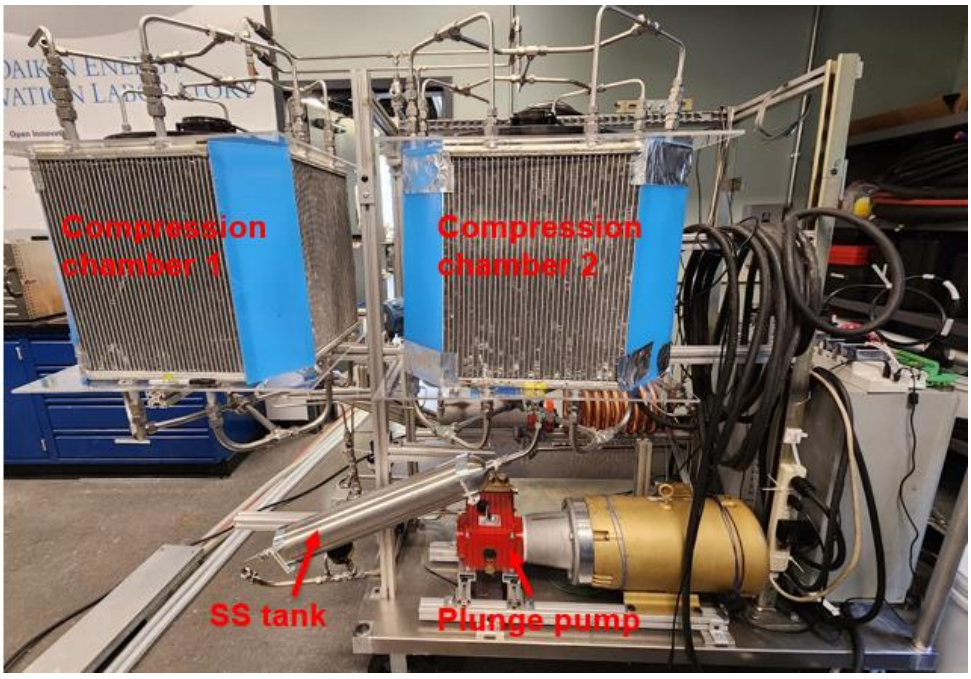

Figure 1: Experimental facility of isothermal compressor

3. MODELING METHODOLOGY

A double-acting liquid piston isothermal compression cycle that has two chambers with shared liquid pump was developed, i.e, either of the compression chamber is endure the suction or compression process and the time period for them are the same. The schematic diagram of the cycle is shown in Figure 2 and following assumptions and explanations are made for modeling.

- A gas cooler is added to the system to further cool the refrigerant delivered from the isothermal compressor and maximize the cooling capacity of the evaporator.
- The accumulator is utilized as storage component to regulate the system charge level and mitigate pressure fluctuation.
- A two-stage pressure regulator is used to control the downstream pressure.
- The electric heater is used as the evaporator to control the suction state of isothermal compressor.

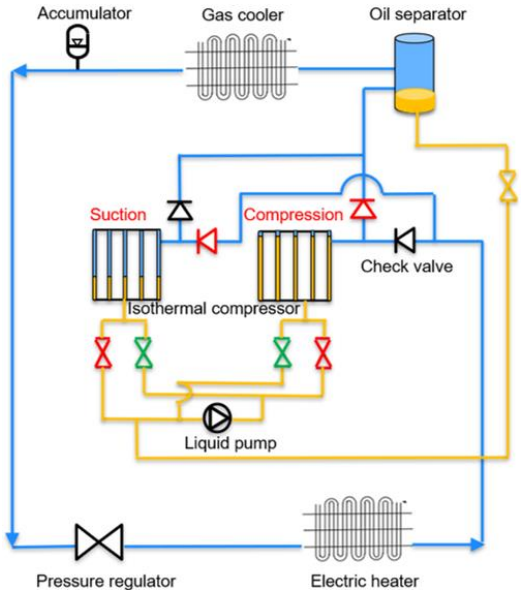

Figure 2: Schematic diagram of isothermal compression system

3.1 Isothermal Compressor with Liquid Piston

The conservation differential equations for the refrigerant energy, mass and tube wall energy for the isothermal compressor are given in Equation 1 to Equation 3.

$$\dot{U} = \dot{m}_{in} h_{in} - \dot{m}_{out} h_{out} - \alpha_r A_r \left(T_r - T_w\right) \tag{1}$$

$$\dot{m}_e = \dot{m}_{in} - \dot{m}_{out} \tag{2}$$

$$\dot{E} = C_{th,w} \dot{T}_w = \alpha_r A_r \left(T_r - T_w\right) - \alpha_a A_a \left(T_w - T_a\right) \tag{3}$$

where U is the refrigerant internal energy; $\dot{m}_{in}$ and $\dot{m}_{out}$ represent the inlet and outlet refrigerant mass flow rates of the chamber, respectively; h_{in} and h_{out} represent the inlet and outlet refrigerant enthalpy of the chamber, respectively; T_r, T_w and T_a are the temperature of refrigerant, chamber wall and surrounding air; $\dot{m}_e$ is the time derivative of refrigerant mass held in the chamber; E is the chamber wall energy and $C_{th,w}$ denotes its thermal capacitance; A_r and A_a are the refrigerant side and air side heat transfer area; α_r and α_a are the refrigerant side and air side heat transfer coefficient (HTC), which are calculated based on Huai et al. (2005) and Chang and Wang (1997) correlations, respectively;

Based on the relationship between the refrigerant internal energy and enthalpy

$$u = h - \frac{P}{\rho} \tag{4}$$

where u is the refrigerant specific internal energy and ρ is the refrigerant density, the time derivative of the refrigerant internal energy U in Equation 1 can be decomposed into terms of time derivatives of the pressure P and enthalpy h using the chain rule:

$$\dot{U} = \left(\frac{\partial \rho}{\partial P} Vh - V\right)\dot{P} + \left(\frac{\partial \rho}{\partial h} Vh + \rho V\right)\dot{h} + \left(\rho h - P\right)\dot{V} \tag{5}$$

where V is the chamber volume of isothermal compressor. Similarly, the mass balance equation of Equation 2 can be rewritten as

$$\dot{m}_e = V\left(\frac{\partial \rho}{\partial P}\dot{P} + \frac{\partial \rho}{\partial h}\dot{h}\right) + \rho\dot{V} \tag{6}$$

Equation 5 and 6 allow the reformulation of the governing equations using the pressure P and enthalpy h as the state variables. The resultant state-space governing equations are

$$\begin{bmatrix} V\frac{\partial \rho}{\partial P}h - V & V\frac{\partial \rho}{\partial h}h + V\rho & 0 & \rho h - P \\ V\frac{\partial \rho}{\partial P} & V\frac{\partial \rho}{\partial h} & 0 & \rho \\ 0 & 0 & C_{th,w} & 0 \\ 0 & 0 & 0 & 1 \end{bmatrix} \begin{bmatrix} \dot{P} \\ \dot{h} \\ \dot{T}_w \\ \dot{V} \end{bmatrix} = \begin{bmatrix} \dot{m}_{in}h_{in} - \dot{m}_{out}h_{out} - \alpha_r A_r\left(T_r - T_w\right) \\ \dot{m}_{in} - \dot{m}_{out} \\ \alpha_r A_r\left(T_r - T_w\right) - \alpha_a A_a\left(T_w - T_a\right) \\ -A_s v \end{bmatrix} \tag{7}$$

where v and A_s are the velocity and the cross-sectional area of liquid piston.

The liquid piston model is simplified as the input to the isothermal compressor, which compresses or suck in the refrigerant within the chamber under the given volumetric flow rate. In our test facility, a mass flow meter was installed at the hydraulic part to measure the volumetric flow rate of oil, and the experimental results were shown in the left part of Figure 3. For modeling purposes, simplifications were thereby implemented: in each process (compression/ suction), the volumetric flow rate was initially kept constant for the first 6 seconds, and then linearly declined throughout the remaining period. Note that the volumetric flow rate profile for each chamber takes mirror relationship.

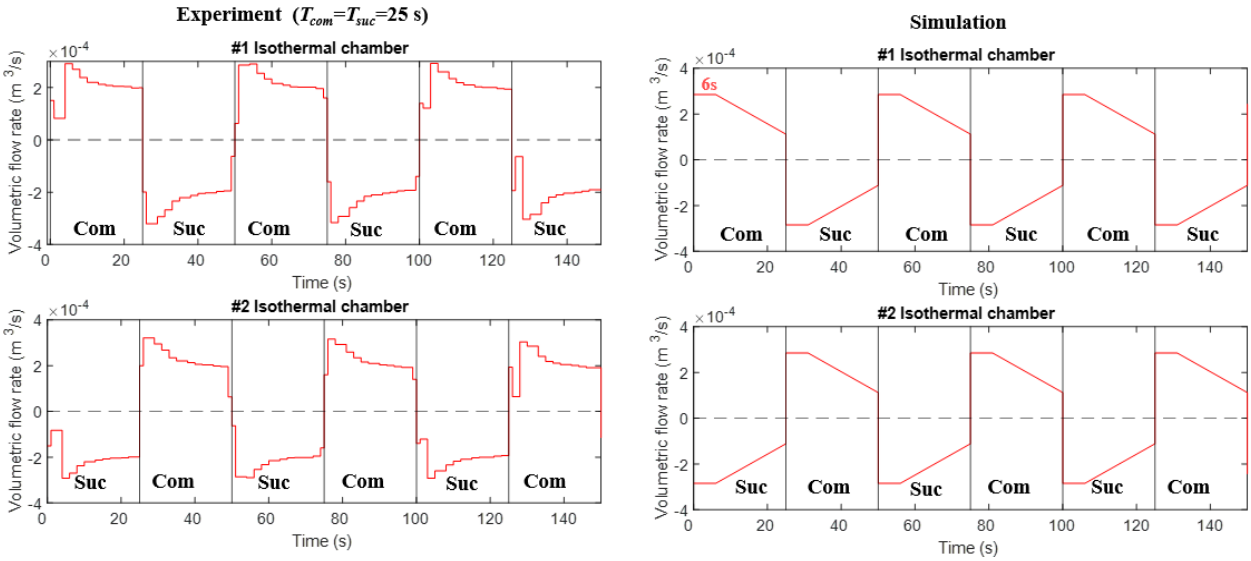

Figure 3: Volumetric flow rate of liquid piston for each compression chamber ("Com": compression, "Suc": suction)

The CO_2 dissolved (compression process) and released (suction process) in the liquid piston medium during the operation is inevitable. Therefore, an appropriate CO_2 solubility correlation can help us find the potential candidate medium for the liquid piston with low solubility and accurately predict the charge level within the isothermal compressor. Amongst many empirical correlations proposed to predict the solubility of CO_2 in oil, we adopted Mehrotra and Svrcek (1982) correlation for predicting CO_2 solubility which is dependent on temperature and saturation pressure as follows:

$$R_s = -0.0073508 - 14.794P_s + 6428.5\left(\frac{P_s}{T}\right) + 4971.39\left(\frac{P_s}{T}\right)^2 \tag{8}$$

where R_s is CO_2 solubility in oil (m^3/m^3); T is the refrigerant temperature and P_s indicates the saturation pressure.

3.2 Gas Cooler with Accumulator, Oil Separator and Connecting Pipe

A tube in tube helical coil is used as the gas cooler to ensure the system reaches to 1-ton cooling capacity. Besides, a diaphragm accumulator model is utilized to stabilize the high side pressure and store the redundant CO_2 during the operation. Few assumptions are made for the modeling:

- There is no heat gain along the refrigerant line connecting the gas cooler and accumulator, i.e., the enthalpy of the accumulator inlet equals that of the gas cooler outlet as this tube section is typically well insulated.
- The oil separator, along with the connecting pipe that links it to the isothermal compressor were also included in the model, which can store quite amount of refrigerant and is regarded as the thermal mass, similarly, this part didn't involve the heat transfer.
- The pressure in the accumulator, as well as in the oil separator and connecting pipe, equals that of the gas cooler due to the lower refrigerant mass flow rate.

The conservation differential equations for the refrigerant mass and energy within the accumulator are:

$$V_f\left(\frac{\partial \rho_N}{\partial P_f}\dot{P}_f + \frac{\partial \rho_N}{\partial h_N}\dot{h}_N\right) = \dot{m}_{acc} \tag{9}$$

$$\left[V_{g_0}-\left(\frac{P_{g_0}V_{g_0}^{n}}{P_g}\right)^{\frac{1}{n}}\right]\dot{P}_f+\beta\dot{V}_f=\beta\dot{V}_{acc} \tag{10}$$

$$P_g=\begin{cases}P_f\left(P_f\geq P_{g_0}\right)\\P_{g_0}\left(P_f<P_{g_0}\right)\end{cases} \tag{11}$$

where N is the number of the control volume in the gas cooler; h_N and ρ_N are the refrigerant outlet enthalpy and density for the gas cooler; $\dot{m}_{acc}$ is the accumulator inlet flow rate; V_f and V_{g0} are the volume for the CO_2 and pre-charged nitrogen in the accumulator, respectively; P_f and P_{g0} are the CO_2 pressure and pre-charged nitrogen pressure in accumulator, respectively; P_g is the nitrogen pressure in the bladder during the operation; β is the bulk modulus of CO_2; n is the polytropic index; $\dot{V}_{acc}$ is the volumetric flow rate of CO_2 suctioned into the accumulator, which is formulated as

$$\dot{V}_{acc}=C_dA\sqrt{\frac{2\left|P_f-P_{g_0}\right|}{\rho_N}}\operatorname{sign}\left(P_f-P_{g_0}\right) \tag{12}$$

where A is the throat area of the accumulator inlet port and the mass flow coefficient C_d is a dimensionless variable that dependents on accumulator's characteristics. Let $\dot{m}_{del}$ be the discharge refrigerant mass flow rate from the isothermal compressor, which relates to the accumulator inlet flow $\dot{m}_{acc}$ via the following equation.

$$\begin{aligned}\dot{m}_{acc}&=\dot{m}_{del}-\underbrace{\left(\dot{m}'_{e,1}+\cdots+\dot{m}'_{e,N}\right)}_{\text{gas cooler}}-\underbrace{\dot{m}'_{e,oil}}_{\text{pipe+oil separator}}=\\&\dot{m}_{del}-\left[V_1\left(\frac{\partial\rho_1}{\partial P_f}\dot{P}_f+\frac{\partial\rho_1}{\partial h_1}\dot{h}_1\right)+\cdots+V_N\left(\frac{\partial\rho_N}{\partial P_f}\dot{P}_f+\frac{\partial\rho_N}{\partial h_N}\dot{h}_N\right)\right]\\&-\left[\left(V_{pipe}+V_{oil}\right)\left(\frac{\partial\rho_1}{\partial P_f}\dot{P}_f+\frac{\partial\rho_1}{\partial h_1}\dot{h}_1\right)\right]\end{aligned} \tag{13}$$

where $\dot{m}'_{e,j}$ (j =1, …, N) and $\dot{m}'_{e,oil}$ represent the time derivative of refrigerant mass held in the gas cooler and connecting pipe with oil separator, respectively; V_{pipe} and V_{oil} represent the refrigerant volume in connecting pipe and oil separator, respectively. By combining the governing equations for the gas cooler, accumulator, oil separator and connecting pipe, an integrated state-space formulation can be obtained as:

$$\begin{bmatrix} -V_1 & V_1\rho_1 & \cdots & 0 & 0 & \cdots & 0 & 0 \\ \vdots & \vdots & \ddots & \vdots & \vdots & \ddots & \vdots & \vdots \\ \sum_{i=1}^{N-1} V_i \frac{\partial \rho_i}{\partial P_f}\left(h_{N-1}-h_N\right)-V_N & V_1 \frac{\partial \rho_1}{\partial h_1}\left(h_{N-1}-h_N\right) & \cdots & V_N\rho_N & 0 & \cdots & 0 & 0 \\ V_f \frac{\partial \rho_N}{\partial P_f}+\sum_{i=1}^{N} V_i \frac{\partial \rho_i}{\partial P_f}+\left(V_{pipe}+V_{Oil}\right)\frac{\partial \rho_1}{\partial P_f} & V_1 \frac{\partial \rho_1}{\partial h_1}+\left(V_{pipe}+V_{Oil}\right)\frac{\partial \rho_1}{\partial h_1} & \cdots & \left(V_f+V_N\right)\frac{\partial \rho_N}{\partial h_N} & 0 & \cdots & 0 & \rho_N \\ 0 & 0 & \cdots & 0 & \left(C_p\rho V\right)_{w,1} & \cdots & 0 & 0 \\ \vdots & \vdots & \ddots & \vdots & \vdots & \ddots & \vdots & \vdots \\ 0 & 0 & \cdots & 0 & 0 & \cdots & \left(C_p\rho V\right)_{w,N} & 0 \\ V_{g_0}-\left(\frac{P_{g_0}V_{g_0}^{\,n}}{P_g}\right)^{\frac{1}{n}} & 0 & \cdots & 0 & 0 & \cdots & 0 & \beta \end{bmatrix} \cdot \begin{bmatrix} \dot{P}_f \\ \dot{h}_1 \\ \vdots \\ \dot{h}_N \\ \dot{T}_{w,1} \\ \vdots \\ \dot{T}_{w,N} \\ \dot{V}_f \end{bmatrix} = \begin{bmatrix} \dot{m}_{del}\left(h_{in}-h_1\right)-\alpha_{i,1}A_{i,1}\left(T_{r,1}-T_{w,1}\right) \\ \vdots \\ \dot{m}_{del}\left(h_{N-1}-h_N\right)-\alpha_{i,N}A_{i,N}\left(T_{r,N}-T_{w,N}\right) \\ \dot{m}_{del}-\dot{m}_{PR} \\ \alpha_{i,1}A_{i,1}\left(T_{r,1}-T_{w,1}\right)-\alpha_{o,N}A_{o,N}\left(T_{w,1}-T_{water,N}\right) \\ \vdots \\ \alpha_{i,N}A_{i,N}\left(T_{r,N}-T_{w,N}\right)-\alpha_{o,1}A_{o,1}\left(T_{w,N}-T_{water,1}\right) \\ \beta C_d A\sqrt{\frac{2\left|P_f-P_{g_0}\right|}{\rho_N}}\,\mathrm{sign}\left(P_f-P_{g_0}\right) \end{bmatrix} \quad (14)$$

where $\dot{m}_{PR}$ is the inlet refrigerant mass flow rate for the pressure regulator; The goodness of helical coil is quantified by an augmentation factor, which is Nusselt number of the helical coil normalized with the Nusselt number of the straight tube at the same Reynolds number and Prandtl number. Therefore, Hardik et al., (2015) correlation was selected to calculate the single-phase HTC for inner and outer part (α_i and α_o) for the helical coil.

Solving the nonlinear differential Equation 14 requires inversion of the transformation matrix, the size of which depends on the number of dynamic states (2*N*+2). To seek a trade-off between the model's prediction accuracy and computational efficiency, the model set was divided into 5 control volumes, i.e., *N*=5. The differential equations were solved numerically using the fourth-order Runge-Kutta solver with a fixed time step of 0.02 s.

3.3 Electric Heater

The electric heater rather than the air source heat exchanger is selected as the evaporator for simplicity concern (no need to consider the air side condition), and it's straightforward to control the predefined superheat by adjusting the heat load directly based on the traditional proportional integral (PI) controller. The PI controlled heat load has the following formulation.

$$Q(n) = K_p T_{sh,e}(n) + K_i \sum_{i=1}^{n} T_{sh,e}(i) \quad (15)$$

where *Q* is the heat load of electric heater in which upper (6,000 W) and lower bound (1,000 W) were provided from the manufacturer; *n* indicates the n^{th} sampling time, K_p and K_i are the (discrete-time) P and I gains of the PI controller, respectively, and $T_{sh,e}$ is the error between the measured superheat $T_{sh,m}$ and its setpoint $T_{sh,s}$. The state-space form of electric heater is similar to that of the gas cooler, except that it utilizes the heater load rather than the air side parameters to account for the heat transfer.

3.4 Pressure Regulator

The pressure regulator is utilized to control the downstream pressure and mass flow rate, where the pressure control relies on the spring force pushing downward against the supply pressure, and the orifice opening varies in accordance with the changes in supply pressure. It is desirable that the controlled pressure does not vary significantly from the setpoint for a wide range of flow rates. Therefore, the following orifice equation is used to calculate the refrigerant flow through the pressure regulator.

$$\dot{m}_{PR} = C_{d,PR} A_{PR} \sqrt{2\rho_{in}\left(P_f - P_e\right)} \tag{16}$$

where A_{PR} is the throat area of the pressure regulator which is determined based on pressure setpoint and ρ_{in} is the inlet refrigerant density; P_f *and* P_e are the upstream and downstream pressure, which are equal to gas cooler and electric heater pressure, respectively; The mass flow coefficient $C_{d,PR}$ is a dimensionless variable which value is provided by manufacturer.

4. EXPERIMENTAL VALIDATIONS

The experimental validation results for the isothermal compression system model were depicted in Figure 4 and 5. As observed in Figure 4, the established model can accurately capture the pressure and temperature behavior of test rig, for both dynamic and steady state characteristics, with 6.2% relative error for the chamber pressure and 0.5 K deviation for the chamber temperature. However, for the pressure part, the simulation curve seems "flatter" than the experimental counterpart, especially at the end of the compression process (delivery of CO_2), which probably because the liquid piston model didn't accurately reflect the real volumetric flow rate during that time. Therefore, one of the future works should be the calibration of liquid piston model. As for the temperature part, a sudden drop at the very beginning of suction process can be observed in the simulation results, which is due to the expansion process of the remained CO_2 in the isothermal chamber. It's noteworthy to mention that although we have retrofitted the experimental setup to narrow down the imbalance between the two chambers, the noticeable difference in the experimental temperature profile is still observable, which may be resulted from the temperature sensor issues.

For the experimental validation of system's high-pressure side (include gas cooler, accumulator, connecting pipe as well as the oil separator), as shown in Figure 5, the established model can accurately capture the behavior of high side pressure overall, i.e, during the early stage of compression process, the gas cooler pressure would be dropped since there is no fed CO_2 from the isothermal compressor, as a contrast, its pressure would be increased because of the delivered CO_2 during the deliver process (later stage of compression process). Note that there is still room for improving the model's accuracy in capturing the system dynamics, which primarily focus on the charge level calibration in the oil separator (no sight glass installed), as this portion of refrigerant can be regarded as the "thermal mass" that affect the system dynamics.

As observed in Figure 5, the evident deviations between simulation and experiment in the suction mass flow rate resulted from our model considering the scenario where a considerable amount of CO_2 would be released during the suction process (pressure decreased), which can't be reflected in the experimental results. As for the discharge mass flow rate, the deviations between simulation and experiment are relatively small.

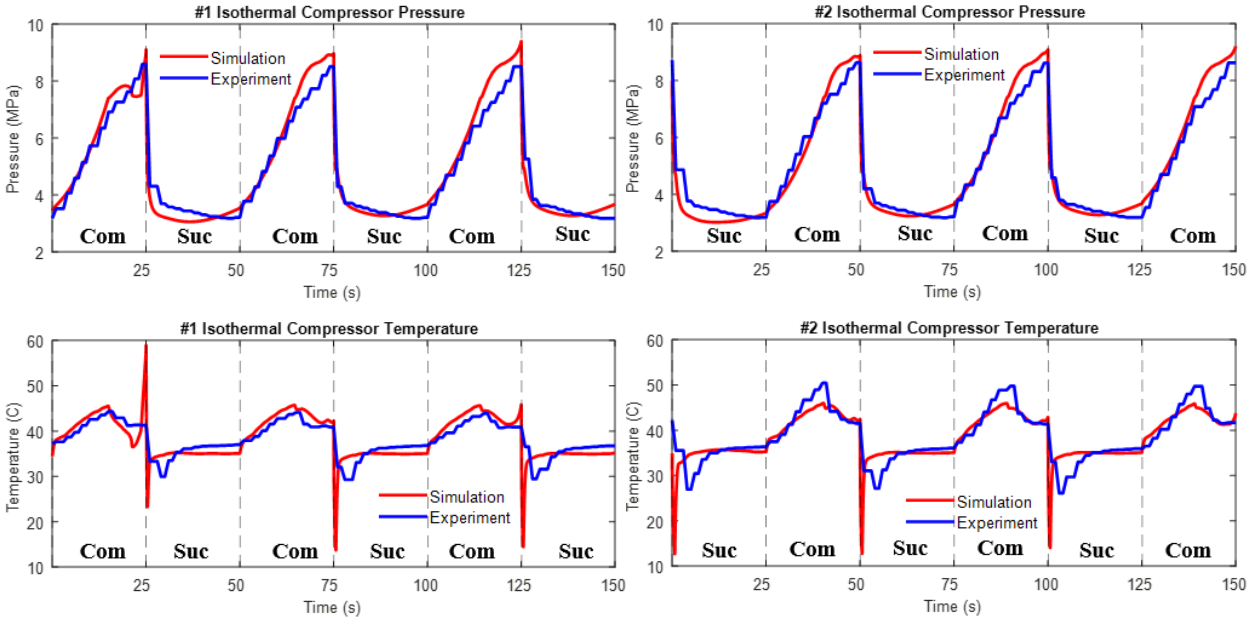

Figure 4: Comparisons of pressure and temperature between experiment and simulation for each compression chamber

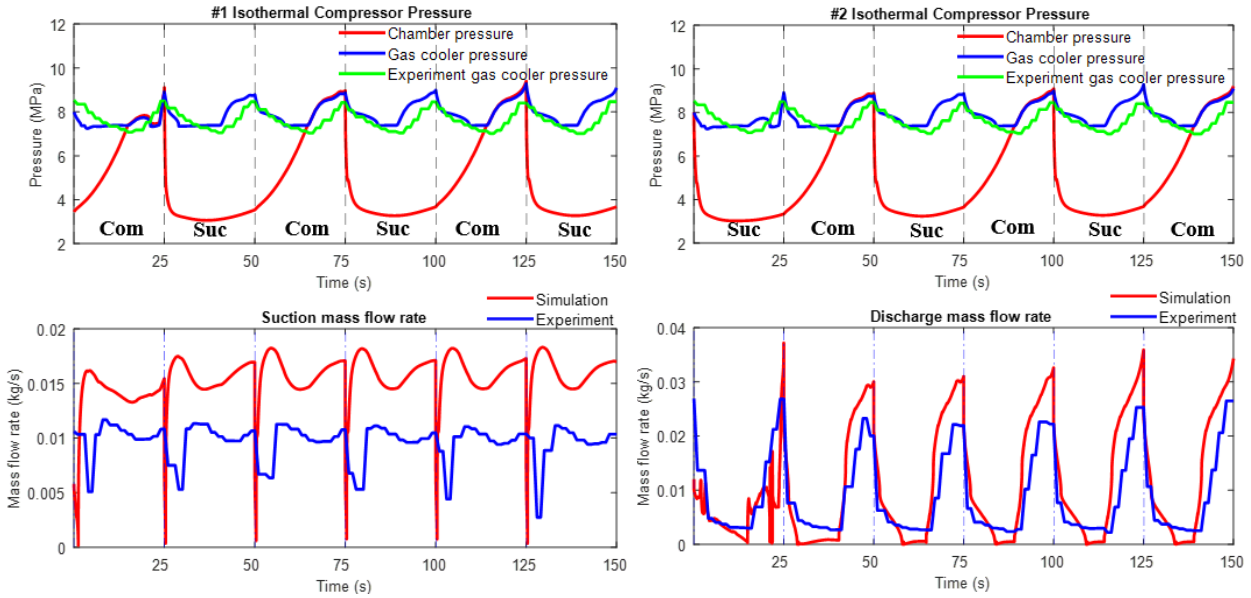

Figure 5: Comparisons of pressure and mass flow rate between experiment and simulation

5. CONCLUSIONS

In this paper, a dynamic model for transcritical CO_2 refrigeration system is established, where the isothermal compressor is coupled with liquid piston to serve the dual purpose as a heat exchanger to cool down the refrigerant and achieve the isothermal compression within the chamber. Unlike the conventional compressor model which evolve on much faster time scales than the heat exchanger dynamics and typically established as quasi-steady state model, the compression process for the isothermal compressor model requires much longer time to dissipate the sufficient heat. The developed isothermal compression cycle is a high fidelity physical-based model that can provide transient behavior of each component in details, furthermore, it also considers the CO_2 solubility phenomenon to better estimate the charge level within system. To demonstrate the accuracy, the experimental tests were carried out with the 1-ton

refrigeration system and the results validated that the established model can accurately capture both the steady-state and dynamic behaviors of test rig (6.2% relative error for chamber pressure and 0.5 K deviation for chamber temperature). The developed model will be used to guide the future design (e.g. shape optimization of chamber) and prototyping, as well as to evaluate the potentials for utilizing the waste heat in the heat recovery applications.

NOMENCLATURE

$\dot{m}$	Mass flow rate	(kg/s)	V_{g0}	Pre-charge volume	(m^3)
U	Refrigerant internal energy	(J)	P_{g0}	Pre-charge pressure	(Pa)
P_e	Electric heater pressure	(Pa)	P_g	Nitrogen pressure in bladder	(Pa)
E	Chamber wall energy	(J)	n	Polytropic index	(–)
T	Temperature	(°C)	C_d	Mass flow coefficient	(–)
P	Pressure	(Pa)	Q	Heat load	(W)
h	Enthalpy	(J/kg)	K_p	P gain of the PI controller	(–)
A	Heat transfer area	(m^2)	K_i	I gain of the PI controller	(–)
V	Volume	(m^3)	$T_{sh,e}$	Superheat error	(K)
R_s	Solubility	(m^3/m^3)	$T_{sh,m}$	Measure superheat	(K)
P_f	Gas cooler pressure	(Pa)	$T_{sh,s}$	Superheat setpoint	(K)
$C_{th,w}$	Wall thermal capacitance	(J/K)	N	number of the control volume	(–)

Greek symbols

α	Heat transfer coefficient	($W/m^2/K$)	β	Bulk modulus	(Pa)
ρ	Density	(kg/m^3)	v	Velocity of liquid piston	(m/s)

Subscript

w	Wall	PR	Pressure regulator
i	Inner	del	Deliver
o	Outer	r	Refrigerant
a	Air	$water$	Chilled water
acc	Accumulator	oil	Oil separator
$pipe$	Connecting pipe		

REFERENCES

EIA (2022). Electricity data. 2022. https://www.eia.gov/energyexplained/electricity/use-of-electricity.php.

Kim, T., Lee, C. Y., Hwang, Y., & Radermacher, R. (2022). A review on nearly isothermal compression technology. *International Journal of Refrigeration*, 144, 145-162.

Qin, C., & Loth, E. (2014). Liquid piston compression efficiency with droplet heat transfer. *Applied Energy*, 114, 539-550.

Patil, V. C., Acharya, P., & Ro, P. I. (2020). Experimental investigation of water spray injection in liquid piston for near-isothermal compression. *Applied energy*, 259, 114182.

Yin, X., Wang, A., Fang, J., Cao, F., & Wang, X. (2021). Coupled effect of operation conditions and refrigerant charge on the performance of a transcritical CO2 automotive air conditioning system. *International Journal of Refrigeration*, 123, 72-80.

Karampour, M., & Sawalha, S. (2018). State-of-the-art integrated CO2 refrigeration system for supermarkets: A comparative analysis. *International journal of refrigeration*, 86, 239-257.

Nawaz, K., Shen, B., Elatar, A., Baxter, V., & Abdelaziz, O. (2018). Performance optimization of CO2 heat pump water heater. *International Journal of Refrigeration*, 85, 213-228.

Wang, J., Belusko, M., Evans, M., Liu, M., Zhao, C., & Bruno, F. (2022). A comprehensive review and analysis on CO2 heat pump water heaters. *Energy Conversion and Management*: X, 15, 100277.

Song, X., Yuan, H., Zhang, Y., Yu, B., Wang, D., Shi, J., & Chen, J. (2022). Experimental study on improved performance of an automotive CO2 air conditioning system with an evaporative gas cooler. *International Journal of Refrigeration*, 140, 39-48.

Kim, T. (2022). Enabling CO2 Isothermal Compression Using Liquid Piston and Integrated Gas Cooler (Doctoral dissertation, University of Maryland, College Park).

Mehrotra, A. K., and Svrcek, W. Y. (1982). Correlations for properties of bitumen saturated with CO2, CH4 and N2, and experiments with combustion gas mixtures. *Journal of Canadian Petroleum Technology*, 21(06).

Huai, X. L., Koyama, S., & Zhao, T. S. (2005). An experimental study of flow and heat transfer of supercritical carbon dioxide in multi-port mini channels under cooling conditions. *Chemical engineering science*, 60(12), 3337-3345.

Chang, Y. J., & Wang, C. C. (1997). A generalized heat transfer correlation for Iouver fin geometry. *International Journal of heat and mass transfer*, 40(3), 533-544.

Hardik, B. K., Baburajan, P. K., & Prabhu, S. V. (2015). Local heat transfer coefficient in helical coils with single phase flow. *International journal of heat and mass transfer*, 89, 522-538.

ACKNOWLEDGEMENT

This material is based upon work supported by the U.S. Department of Energy's Office of Energy Efficiency and Renewable Energy (EERE) under the Building Technologies Office Award Number DE-EE0008674.